OPTO-ELECTRONICS REVIEW **8**(2), 129–135 (2000)

Complex refractive index concept for the description of sevanescent wave sensor

J. RAYSS* and G. SUDOLSKI

Laboratory of Optical Fibre Technology, Faculty of Chemistry, M.C. Skłodowska University
3 Sq. M.C. Skłodowska, 20-031 Lublin, Poland

The paper presents the analysis of the multimode fibre optic evanescent wave sensor response. Theoretical considerations, based on losses during the single reflection and the complex refractive index, showed non–linearity between the sensor response (absorbance) and the imaginary part of the refractive index, hence, concentration of examined species. To confirm the theoretical predictions, an experiment in the model sensor set–up was performed. As an absorbing species amidoblack dye (naphtol blue black) was used. Good agreement between the experimental results and theoretical predictions was observed.

Key words: evanescent wave, complex refractive index, fibre optic sensor, amidoblack dye.

1. Introduction

Evanescent wave sensors become more and more widespread [1,2] although the response of the sensors depends on many parameters, i.e., kind of applied fibre, light source, detector system, sensor geometry [3,4]. Theoretical description of the evanescent wave sensor can be based either on the mode analysis or the geometric optics. The mode analysis can potentially give an exact sensor description, but needs complicated mathematical methods and even for a few mode fibres many simplifications have to be applied (weakly guiding, steady state). The geometric optics exploits simpler expressions than the modal analysis, but it is shortcoming for the angles close to the critical angle and neglects leaky rays, which, in turn, interact strongly as the evanescent wave giving the greatest contribution to the total sensor signal. The approach combining the geometric optics and the complex refractive index concept presented in this paper makes it possible to describe the evanescent wave sensor response even for the states far from the steady one.

2. Theory

2.1. Single reflection at dielectric interface

The light ray incident on interface of dielectrics splits into two rays, the refracting ray and reflecting one. Treating individual rays as plane waves and considering x-component only (Fig. 1), we obtain

$$\Psi_{i,x} = A e^{ik_{i,x}x} = A e^{ikn_1 \sin\theta_z x - i\omega t}, \quad (1a)$$

$$\Psi_{r,x} = B e^{ik_{r,x}x} = B e^{-ikn_1 \sin\theta_r x - i\omega t}, \quad (1b)$$

$$\Psi_{t,x} = C e^{ik_{t,x}x} = C e^{ikn_2 \sin\theta_t x - i\omega t}, \quad (1c)$$

where Ψ_i, Ψ_r, Ψ_t, A, B, and C, are the wave functions and amplitudes corresponding to the incident, reflected, and refracted rays, respectively; k' is the wave number ($k' = 2\pi n/\lambda$, n is the refractive index), ω is the angular frequency; θ_z, θ_r, θ_t are the angles complementary to the incident, reflecting, and refracting angles, respectively. In further considerations time dependence $e^{-i\omega t}$ is omitted for simplification. Angles θ_t and θ_z are not independent, but they are related according to the Snell's law [5]

$$\cos\theta_t = \frac{n_1}{n_2}\cos\theta_z. \quad (2)$$

The continuity condition of the wave functions and their first derivative at x = 0 lead to the relationship between amplitudes of the individual rays known as Fresnel's equation [6]. This equation do not take into account the polarisation state of the incident ray. Such simplification can be acceptable in the case of non-coherent light source (lack of distinguished direction of polarisation) or when $n_2 \cong n_1$ (weakly guiding approximation):

$$\frac{B}{A} = \frac{n_1 \sin\theta_z - n_2 \sin\theta_t}{n_2 \sin\theta_t + n_1 \sin\theta_z}, \quad (3a)$$

$$\frac{C}{A} = \frac{2 \cdot n_1 \sin\theta_z}{n_2 \sin\theta_t + n_1 \sin\theta_z}. \quad (3b)$$

When $n_2 < n_1$ and $\theta_z < \arccos(n_2/n_1)$ total internal reflection occurs and $\cos\theta_t$ becomes imaginary that can be written as

$$\sin\theta_t = i\sqrt{\frac{n_1^2}{n_2^2}\cos^2\theta_z - 1}, \quad \frac{n_1^2}{n_2^2}\cos^2\theta_z > 1, \quad (4)$$

*e-mail: koper@hermes.umes.lublin.pl

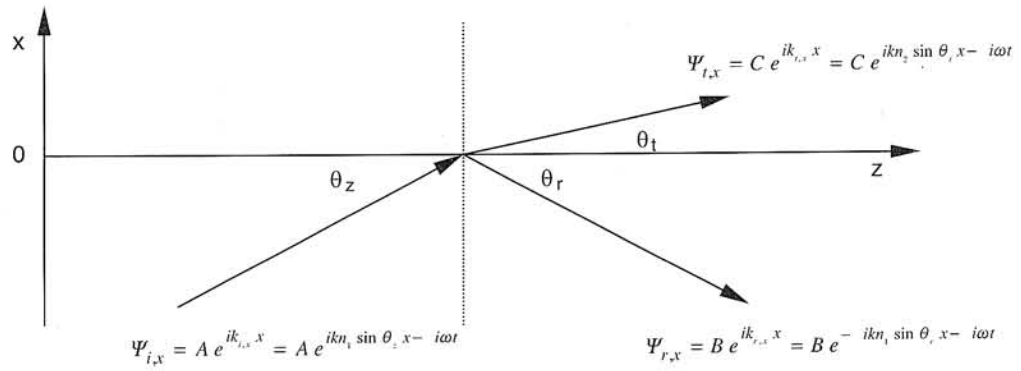

Fig. 1. Incident, reflecting, and refracting rays with corresponding wave functions.

and it corresponds to the wave function of the refracted ray in the form

$$\Psi_{i,x} = C \exp\left(- kn_1 \sqrt{\cos^2\theta_z - \frac{n_2^2}{n_1^2}}\; x \right). \tag{5}$$

Equation (5) shows that amplitude of the refracting ray, during the total internal reflection, decays exponentially with the distance from the interface of the dielectrics. This phenomenon is referred to the evanescent wave. Change of the refractive ray into the evanescent wave with variation of θ_z, when the total internal reflection is allowed ($n_2 < n_1$), is illustrated in Fig. 2.

The full form of the evanescent wave is obtained by taking z-component into account, as well

$$\Psi_{t,x,z} = C \exp\left(- kn_1 \sqrt{\cos^2\theta_z - \frac{n_2^2}{n_1^2}}\; x + ikn_1 \cos\theta_z\, z \right). \tag{6}$$

It follows from Eq. (6) that the evanescent wave propagates along the z-axis direction, but is decaying into the optically rarer medium, parallel to the x-axis direction (see Fig. 3) [7].

To characterise the evanescent wave a penetration parameter was introduced. The penetration depth d_p is defined as a distance, into the optically rare medium, at which an amplitude of the evanescent wave decreases to 1/e of its initial value and can be given by

$$d_p = \frac{\lambda}{2\pi n_1 \sqrt{\cos^2\theta_z - \left(\frac{n_2}{n_1}\right)^2}}$$

or

$$d_p = \frac{\lambda}{2\pi n_1 \sqrt{\sin^2\theta_c - \sin^2\theta_z}}, \tag{7}$$

where θ_c is the angle complementary to the critical angle, defined as

$$\theta_c = \arccos\frac{n_2}{n_1}, \quad n_2 < n_1. \tag{8}$$

For the fused silica (n = 1.458)/water (n = 1.333) system and for VIS range (380–780 nm) the average value of d_p is about 250 nm, but for the angles close to the critical angle d_p exceeds even 1 μm. This is much more than mo-

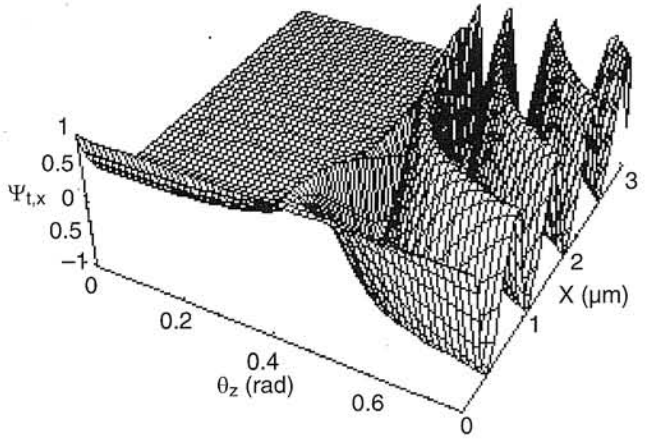

Fig. 2. Wave function of the refracting ray $\Psi_{t,x}$ drawn for n_1 = 1.458, n_2 = 1.334, λ = 0.589 μm, $\theta_c \approx 0.4$ rad, and C = 1. For the angles θ_z smaller than θ_c the function $\Psi_{t,x}$ decays exponentially (evanescent wave), however, for $\theta_z > \theta_c$ the function $\Psi_{t,x}$ has a wave character.

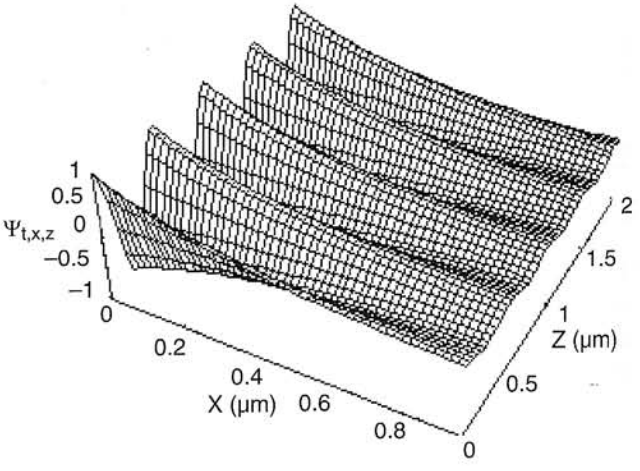

Fig. 3. Function representing the evanescent wave ($\Psi_{t,x,z}$). The plane drawn for n_1 = 1.458, n_2 = 1.334, λ = 0.589 μm, θ_z = 0.36 rad, and C = 1.

lecular dimensions and enables recording spectra of the species present in an optically rare medium, which is a basis for the well known technique referred to the attenuated total reflectance spectroscopy (ATR).

Apparently, for the total internal reflection the expressions analogous to the Fresnel's equations become complex and can be given in the form [6]

$$\frac{B}{A} = \frac{\sin\theta_z - i\sqrt{\cos^2\theta_z - \frac{n_2^2}{n_1^2}}}{\sin\theta_z + i\sqrt{\cos^2\theta_z - \frac{n_2^2}{n_1^2}}}, \tag{9a}$$

$$\frac{C}{A} = \frac{2\sin\theta_z}{\sin\theta_z + i\sqrt{\cos^2\theta_z - \frac{n_2^2}{n_1^2}}}. \tag{9b}$$

Since light intensity is proportional to the square of wave amplitude [8], thus, energy transmitted across the interface T at single reflection is equal to

$$T = 1 - \left(\frac{B}{A}\right)^2. \tag{10}$$

If we substitute equation (9a) into (10), we obtain [6]:

$$T = \frac{4\sin\theta_z \,\mathrm{Re}\sqrt{\frac{n_2^2}{n_1^2} - \cos^2\theta_z}}{\left|\sin\theta_z + \sqrt{\frac{n_2^2}{n_1^2} - \cos^2\theta_z}\right|^2}$$

or alternatively

$$T = \frac{4\sin\theta_z \,\mathrm{Re}\sqrt{\sin^2\theta_z - \sin^2\theta_c}}{\left|\sin\theta_z + \sqrt{\sin^2\theta_z - \sin^2\theta_c}\right|^2} \tag{11}$$

Since $\mathrm{Re}\sqrt{n_2^2/n_1^2 - \cos^2\theta_z} \neq 0$ only for $\theta_z > \theta_c$, relationship (11) refers only to the refractive rays (see Fig. 4). The line depicted in Fig. 4 confirms the well-known fact that energy is not transmitted (T = 0) for the angles $\theta_z < \theta_c$ when the total internal reflection is allowed ($n_2 < n_1$).

Equation (11) describes refraction losses only and does not take into account absorption properties of both optically rarer and denser media. This shortcoming can be overcome by introducing the complex refractive index, which is defined as [9,10]

$$n^2 = \mu\left(\varepsilon + i\frac{\sigma}{\omega\varepsilon_0}\right), \tag{12}$$

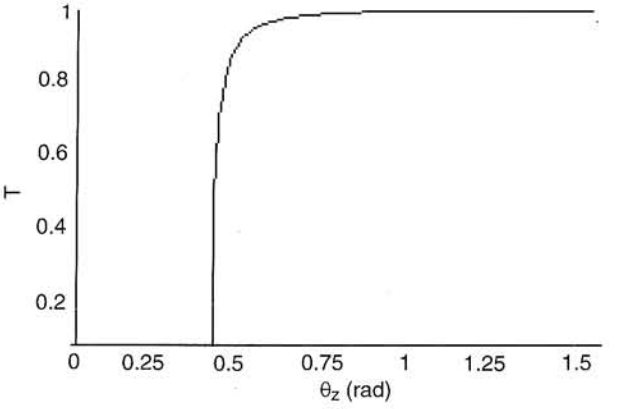

Fig. 4. Relationship between the energy transmission coefficient (T) and θ_z for the fused silica glass (n_1 = 1.458)/water (n_2 = 1.334) and $\theta_c \approx 0.4$ rad.

where μ is the magnetic permittivity, ε is the dielectric constant, ε_0 is the electric permittivity of the vacuum, σ is the electric conduction of the medium, and ω is the angular frequency.

For many media (except ferrimagnetics) $\mu \approx 1$ and at the assumption that the medium under consideration does not conduct ($\sigma = 0$), Eq. (12) gives the well known relationship

$$n^2 = \varepsilon. \tag{13}$$

As a matter of fact, light is an electromagnetic wave having enormous frequency (for VIS range $\omega \approx 10^{16}$ Hz) which causes electron oscillations which, in turn, can be interpreted as intermolecular current despite the fact that the medium lacked conductivity (on condition that the wave energy is not sufficient to ionise atoms or molecules and produces free current carriers). In such conditions an imaginary part of the refractive index is manifesting. Intensity of the intermolecular current depends on the resonance frequency of electrons in the atom or molecule. It means that value and wavelength characteristic of the imaginary part is an inherent feature of the examined species.

Accordingly, the complex refractive index can be attributed to every dielectric medium in the form

$$n = n_{re} + in_{im}. \tag{14}$$

Applying Eq. (14) to a wave equation, we obtain

$$\Psi = A_\Psi e^{iknx} = A_\Psi e^{ik(n_{re}+in_{im})x} = A_\Psi e^{kn_{im}x} e^{ikn_{re}x}, \tag{15}$$

where an amplitude of the wave decreases exponentially and decay is governed by an imaginary part of the refractive index. Expression (15) describes the attenuated wave with the attenuation coefficient n_{im}. Introducing the complex refractive index into Eq. (11), we obtain

$$T = \frac{4\sin\theta_z \,\mathrm{Re}\sqrt{\frac{(n_{2,re}+in_{2,im})^2}{(n_{1,re}+in_{1,im})^2} - \cos^2\theta_z}}{\left|\sin\theta_z + \sqrt{\frac{(n_{2,re}+in_{2,im})^2}{(n_{1,re}+in_{1,im})^2} - \cos^2\theta_z}\right|^2}. \tag{16}$$

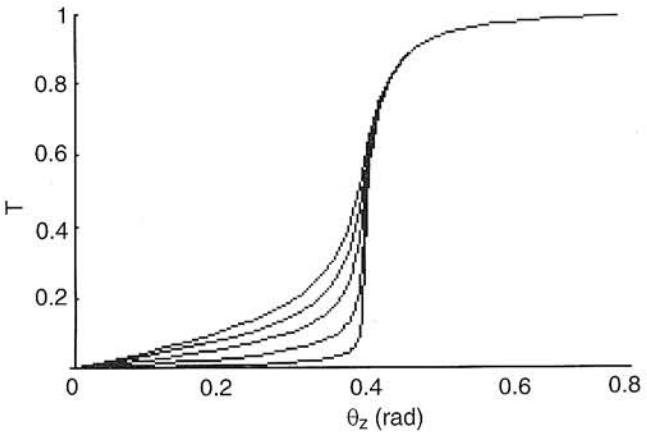

Fig. 5. The energy transmission coefficient (T) vs. angle θ_z for the following values of the parameters: $n_{1,re} = 1.458$, $n_{1,im} = 0$; $n_{2,re} = 1.334$, $n_{2,im} = 1\times10^{-3}, 3\times10^{-3}, 6\times10^{-3}, 9\times10^{-3}, 12\times10^{-3}$.

Assuming $n_{1,im} = 0$ and $n_{2,im} \neq 0$, that correspond to the case when only the optically rare medium is absorbing one, the relationship between the transmission energy coefficient T and θ_z differs from those in Fig. 4. The energy transmission T has non-zero values even for the angles satisfying conditions of the total internal reflection (see Fig. 5). It means that the amplitude/intensity of the reflected ray is smaller than that of the incident one.

2.2. Multiple total internal reflection at a multimode fibre waveguide

A light ray transmitted in a multimode waveguide undergoes multiple total internal reflection, moreover, there are propagated rays reflected at various incident angles. Additionally, skew rays, which never cross the fibre axis, should be taken into account. Skewness is determined by the angle θ_ϕ in the core cross-section between the tangent to the interface and projection of the ray path (Fig. 6).

Light intensity variations with the distance z of the fibre and the angles θ_z, θ_ϕ are described by [6,13]:

$$I(\theta_z,\theta_\phi,z) = I_0(\theta_z,\theta_\phi)\, e^{-\gamma(\theta_z,\theta_\phi)z} \tag{17}$$

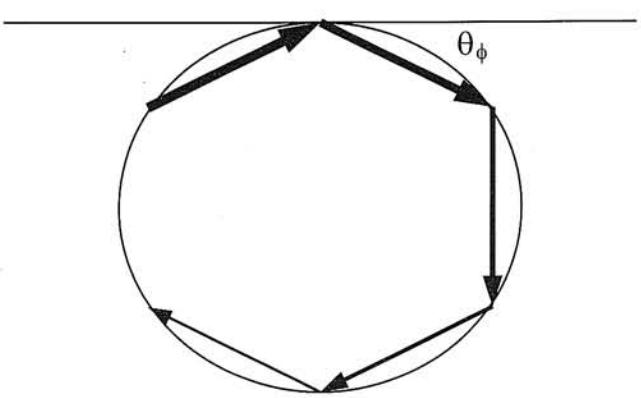

Fig. 6. Skew ray in a fibre waveguide.

where $I_0(\theta_z, \theta_\phi)$ and $I(\theta_z, \theta_\phi, z)$ are the intensity distribution at fibre input and output, respectively; $\gamma(\theta_z, \theta_\phi)$ is the absorption/extinction coefficient related to the energy transmission coefficient T according to $\gamma(\theta_z, \theta_\phi) = T(\theta_z, \theta_\phi)N(\theta_z, \theta_\phi)$, where $N(\theta_z, \theta_\phi)$ is the number of reflections per unit length that can be expressed as

$$N = \frac{tg\theta_z}{2a\sin\theta_\phi} \tag{18}$$

where a is the radius of the fibre core.

During the spectroscopic measurement the average value of light intensity, corresponding to a certain range of angles, is recorded. The obtained result can be presented in form of the absorbance E_m that compares light intensity during reference P_{ref} and sample measurement P_s according to

$$E_m = \log\frac{P_{ref}}{P_s} \tag{19}$$

where

$$P_{ref} = \frac{\int\int I_0(\theta_z,\theta_\phi)\, e^{-N(\theta_z,\theta_\phi)T_{ref}(\theta_z,\theta_\phi)z}\, d\theta_z d\theta_\phi}{\int\int I_0(\theta_z,\theta_\phi) d\theta_z d\theta_\phi} \tag{20}$$

$$P_s = \frac{\int\int I_0(\theta_z,\theta_\phi)\, e^{-N(\theta_z,\theta_\phi)T_s(\theta_z,\theta_\phi)z}\, d\theta_z d\theta_\phi}{\int\int I_0(\theta_z,\theta_\phi) d\theta_z d\theta_\phi} \tag{21}$$

Limits of the integrals are related to the geometry of the detecting system.

Since the reference measurement is usually carried out in the absence of absorbing species ($\gamma_{ref} = 0$), absorbance can be evaluated according to

$$E_m = \log\frac{\int\int I_0(\theta_z,\theta_\phi) d\theta_z d\theta_\phi}{\int\int I_0(\theta_z,\theta_\phi)\, e^{-N(\theta_z,\theta_\phi)T_s(\theta_z,\theta_\phi)z}\, d\theta_z d\theta_\phi} \tag{22}$$

In this point, it must be emphasised that energy transmission coefficient T was obtained assuming that the propagating rays are plane waves and, in consequence, Eq. (22) is valid only for the multimode fibres for which such an approximation is allowed. On the basis of Eqs. (22) and (16), theoretical lines were drawn and the results are shown in Fig. 7.

The results of theoretical calculations show that for not large values of $n_{2,im}$ the function is linear and satisfies the Lambert-Beer's law. However, for higher values of an imaginary part of the refractive index greater and greater deviation from linearity is observed. Quantitatively, the obtained theoretical results are comparable to the investigations made by other authors exploiting the modal analysis [12,13]. There must be taken a note of the fact that an imaginary part of the refractive index is related to the species concentration and its molar absorption coefficient, as follows [6]:

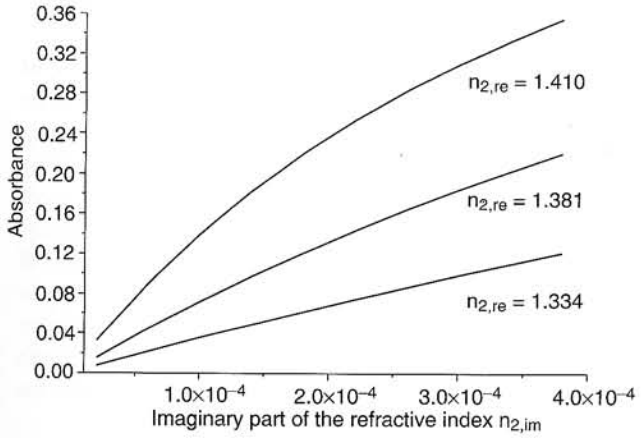

Fig. 7. Relationship between the absorbance (E_m) of the evanescent wave and an imaginary part of the refractive index ($n_{2,im}$) of a medium surrounding fibre core. The lines drawn according to Eqs. (22) and (16) for given values of the parameters: $n_{2,re}$ = 1.410, $n_{2,re}$ = 1.381, $n_{2,re}$ = 1.334, $n_{1,re}$ = 1.458, $n_{1,im}$ = 0; $I_o(\theta_z)$ = $\cos(\theta_z*\pi/2*1/NA)$ [6], NA = 0.55 [11], z = 35 cm, a = 100 μm.

$$n_{im} = \frac{c\varepsilon\lambda}{4\pi}, \tag{23}$$

where c is the molar concentration of examined species, ε is the molar absorption coefficient at the wave length λ.

The result presented in Fig. 8 indicates that the increase in the refractive index of the cladding, more generally of the medium surrounding core, causes increase in absorbance. Non-linearity of this phenomenon enables increase in absorbance and in consequence in sensor sensitivity.

3. Experiment

3.1. Materials

The standard PSC fibre (core diameter 200 μm and NA ≈ 0.38), produced in the Laboratory of Optical Fibre Technology UMCS, was used. Fibre cladding, silicon rubber,

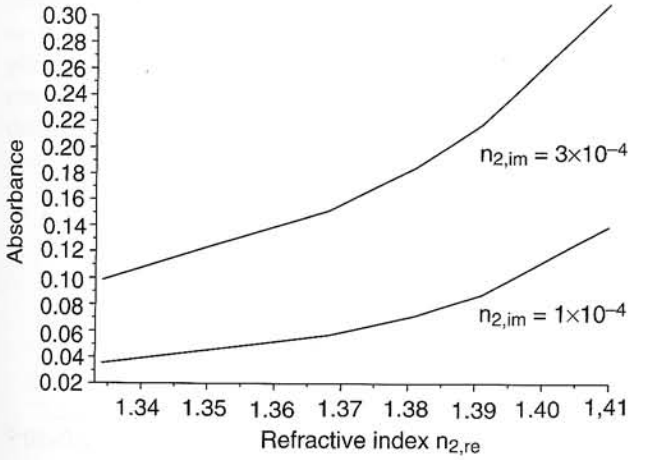

Fig. 8. Theoretically calculated evanescent wave absorbance vs. refractive index of the medium surrounding the fibre core. Lines drawn for given values of an imaginary part of the refractive index.

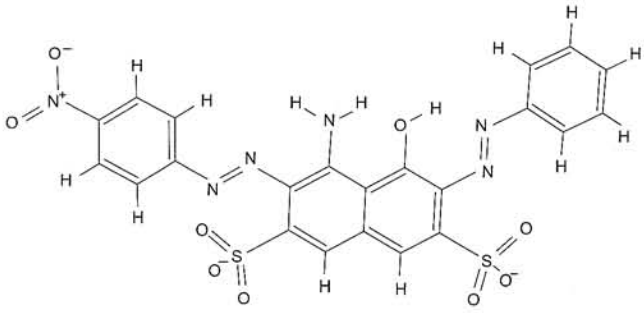

Fig. 9. Structural formula of the amidoblack (naphtol blue black).

was removed by means of a surgical blade after the treatment with the mixture of acetone and ethylene chloride (1:1 v/v). A 35-cm long section deprived of cladding was coiled into two loops 6.5 cm in diameter. The fibre was held in the laboratory made Teflon support. Fibre length between sensing section and both light source and detector was constant and equal to 55 cm.

Solutions at different refractive indices (in the range of 1.333–1.410) were prepared by mixing appropriate volumes of water and glycerine (POCh, Gliwice, Poland, analytically pure). Every time the refractive index was measured by the Abbe's refractometer (RL-2, PZO Warszawa, Poland). As the absorbing species the amidoblack, see Fig. 9, (Fluka, Germany) was chosen because of high absorption coefficient and good solubility in water. Amidoblack solutions at the concentration range 2×10^{-5} mol/dm^3 do 2×10^{-3} mol/dm^3 were prepared.

3.2. Spectrophotometric measurements

The spectra of amidoblack in water (n = 1.334) as well as in glycerine solutions (n = 1.410) were recorded by means of the double beam spectrophotometer (Specord, M40, Karl Zeiss Jena) using 0.1 cm cuvettes (Fig. 10). According to the obtained spectra the molar extinction/absorption coefficient of the dye was calculated. In a broad range of concentrations the molar absorption co-

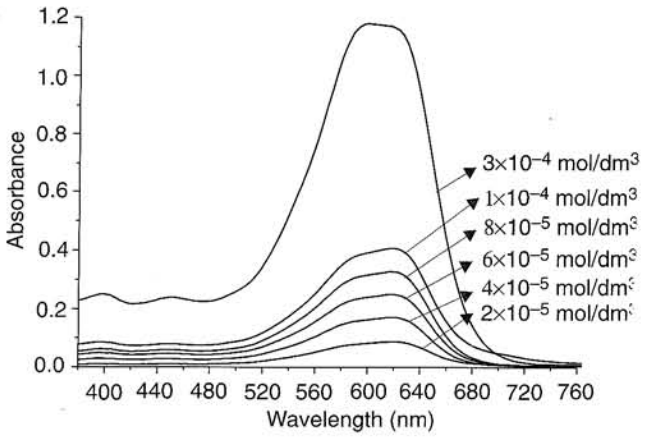

Fig. 10. Examplary spectra of amidoblack for different dye concentrations. Measurements were made using the 0.1-cm cuvette.

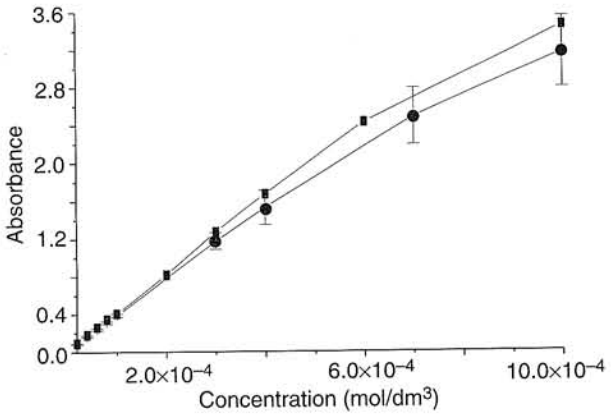

Fig. 11. Relationship between absorbance of the amidoblack solutions at λ = 630 nm and concentration of the dye, ■ – the glycerine solutions, ● – the water solutions.

efficient was constant and equal to $\alpha_{\lambda=630\ nm} \approx 4\times10^4$ $dm^3mol^{-1}cm^{-1}$ (Fig. 11), even though slight deviations from linearity were observed for more concentrated solutions. This case corresponded to very high values of absorbance, hence, a relatively large measurement error. Glycerine solutions showed slightly higher values of the molar absorption coefficient.

3.3. Measurements in the evanescent wave system

As a light source white LED, having a spectral range from 420 to 720 nm and NA ≈ 0.65, was used. Detection was performed using the fibre optic spectrophotometer SPM-14 (WOCAD, Poland) that featured the spectral range of 380–780 nm, resolution 7 nm, and scanning fibre (core diameter 50 μm and NA = 0.22). Scheme of the measurement set-up is shown in Fig. 12.

Due to the angular relationship of evanescent wave absorbance, the scanning fibre was placed in the position corresponding to 90% maximal recorded intensity. Such a procedure was applied as a compromise, on one hand at smaller angles smaller absorbance was expected, on the other hand at larger angles the lower signal level leads to the worse signal-to-noise ratio. However, the fibre coupling procedure made it possible to obtain reproducible and comparable results.

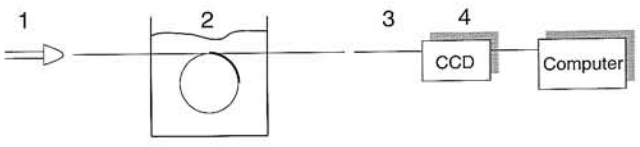

Fig. 12. Scheme of the measurement set-up.
1. White LED NA ≈ 0.65, 2. Sensing section of the fibre immersed into the amidoblack solutions, 3. Scanning fibre (50/125 μm, NA 0.22) – the integral part of the spectrophotometer, 4. CCD fibre optic spectrophotometer

4. Results and discussion

In Fig. 13, the examples of evanescent wave spectra of amidoblack water solutions are shown. The shape of the lines differ slightly from those obtained in the cuvette, but the maximum of absorption band occurred in the same range of the wavelength, namely 620–640 nm. For further investigations, aiming at finding the relationship between the evanescent wave absorbance and the dye concentration, wavelength at λ = 630 nm was chosen. The obtained results are drawn in Fig. 14. However, dependence of absorbance on the refractive index of a given dye concentration is shown in Fig. 15. Both shapes and absorbance values show good agreement with the theoretical predictions (see Figs. 7 and 8).

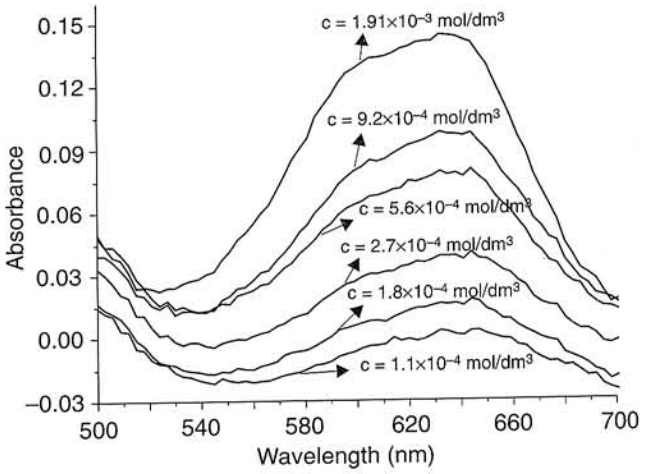

Fig. 13. Evanescent wave spectra of amidoblack in water solutions. Spectra recorded at different dye concentrations.

Comparison of the theoretically calculated absorbance and the experimental one is shown in Fig 16. An imaginary part of the refractive index for the experimental points was calculated according to Eq. (21).

The diagrams show that theoretical predictions underestimate the experimental points. These slight discrepancies

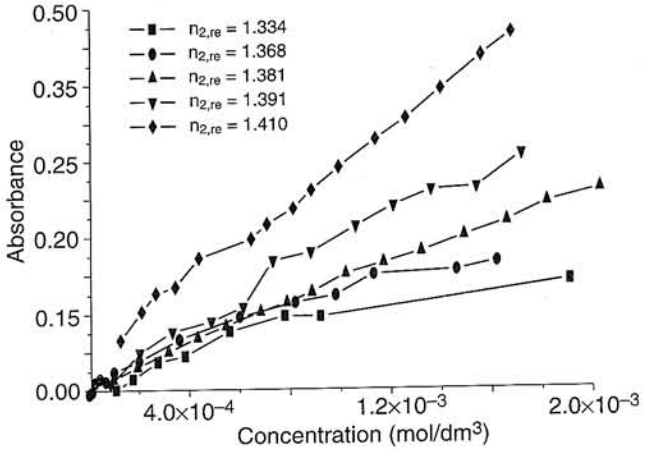

Fig. 14. Results of measurements recorded at λ = 630 nm for different refractive indices and concentrations of amidoblack solutions.

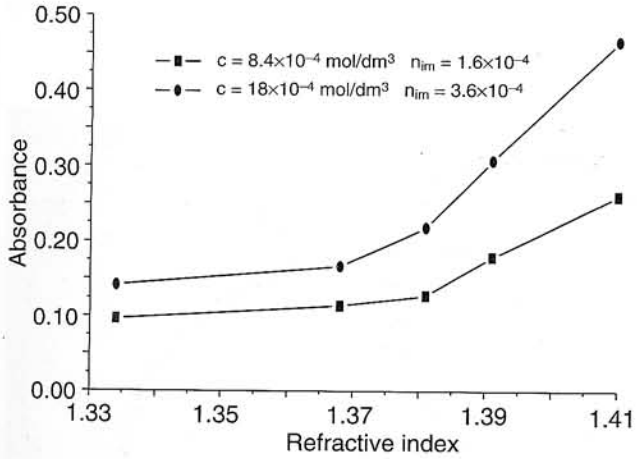

Fig. 15. Dependence of evanescent wave absorbance on the refractive index for the chosen values of amidoblack concentrations.

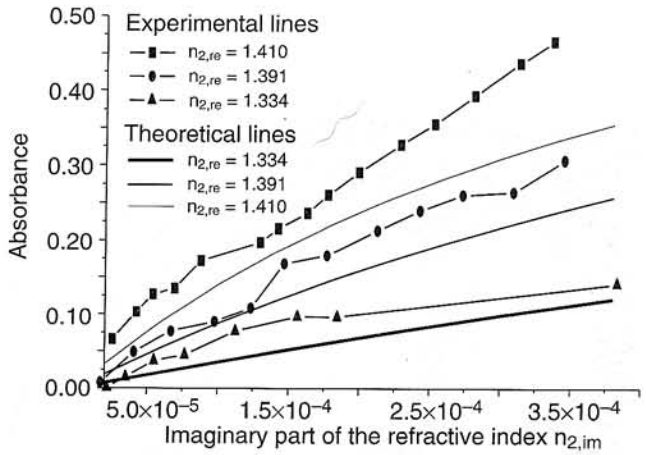

Fig. 16. Comparison of the experimental evanescent wave absorbance and the theoretical one of selected values of the refractive indices. Dotted lines – experimental results, solid lines – theoretical predictions.

between the experimental points and the theoretical lines can result from the fact that fibre coiling was not taken into consideration. In the curved fibre the angular ray distribution differed from the assumed one. Another reason for the disagreement between the theoretical predictions and the experimental results can be adsorption of the dye molecules which brings about a local increase of the dye concentration in the space near the fibre core.

To compare the cuvette and the evanescent wave results it is convenient to define evanescent wave molar extinction coefficient in the form

$$\varepsilon_{ev} = \frac{E_{ev}}{cl} \tag{24}$$

where l is the length of the fibre sensing section, it turns out that its value is about 3 $dm^3mol^{-1}cm^{-1}$, i.e., 10000 times less than the "normal" molar extinction coefficient. It means that the proposed sensing system based on the evanescent wave absorption can be applied for the on-side and on-line determination of colourful solution without sampling and sample dilution. Another aspect, that should be emphasised, is increase of ε_{ev} with the refractive index increase. This phenomenon might be useful in the analytical practice.

References

1. C. Egami, K. Takeda, M. Isai, and M. Ogita, *Opt. Commun.* **122**, 122 (1996).
2. P. Radhakrishnan, V.P.N. Nampoori, and C.P.G. Vallabhan, *Opt. Eng.* **32**, 692 (1993).
3. T.B. Colin, K.H. Yanh, M. A.Arnold, G.M. Small, and W.C. Stwalley, *Appl. Spectrosc.* **46**, 1129 (1992).
4. B.D. Gupta, C.D. Singh, and A. Sharma, *Opt. Eng.* **33**, 1864 (1994).
5. J. Petykiewicz, *Wave Optics*, PWN, Warsaw, 1986. (in Polish).
6. A.W. Snyder and J.D. Love, *Optical Waveguide Theory*, Chapman & Hall, London, 1983.
7. J. Petykiewicz, *Fundamentals of Integrated Optics*, PWN, Warsaw, 1989. (in Polish).
8. A. Januszajtis, *Physics for Students of University of Technology*, Vol. 3, "Waves", PWN, Warsaw, 1991. (in Polish).
9. A.J. Wojtowicz, *Lecturers on General Physics*, Optics, "Integrated refractive index", www.phys.uni.torun.pl/~andywojt/wyklady/wyklad10/wyklad10.html (in Polish).
10. R.P. Feynman, R.B. Leighton, and M. Sands, *Feynman's Lecturers on Physics*, Vol. 1, Part 2, PWN, Łódź, 1971. (in Polish).
11. J. Rayss and G. Sudolski, "Dependence of signal of evanescent wave sensor on its length and refractive index of medium", *VII Conf. on Fibres and Their Applications*, Krasnobród, 1999, Tom II (1999) 374. (in Polish).
12. V. Ruddy, *Opt. Eng.* **33**, 3891 (1994).
13. F.P. Payne and Z.M. Hale, *Int. J. Optoelectr.* **8**, 743 (1993).